

Article

Fabrication of Reduced Ag Nanoparticle Using Crude Extract of Cinnamon Decorated on ZnO as a Photocatalyst for Hexavalent Chromium Reduction

Intan Nurul Rizki ^{1,*}, Takumi Inoue ², Chitiphon Chuaicham ², Sulakshana Shenoy ², Assadawoot Srikaow ², Karthikeyan Sekar ² and Keiko Sasaki ^{2,*}

¹ Nanotechnology Engineering, Faculty of Advanced Technology and Multidiscipline, Airlangga University, Surabaya 60115, Indonesia

² Department of Earth Resources Engineering, Kyushu University, Fukuoka 819-0395, Japan

* Correspondence: intan.nurul@ftmm.unair.ac.id (I.N.R.); keikos@mine.kyushu-u.ac.jp (K.S.)

Abstract: The crude extract of cinnamon (after abbreviated as KM) was used to produce silver nanoparticles (AgKM). This was subsequently utilized for the hydrothermal production of a composite consisting of AgKM decorated on zinc oxide (AgKM/ZnO) as a photocatalyst for reducing hexavalent chromium (Cr(VI)). Several methods e.g., XRD, SEM, TEM, XPS, PL, and RDB-PAS were used to analyze the optical and physicochemical properties of ZnO/AgKM samples in order to better comprehend the impact of the development of the AgKM-ZnO heterojunction in comparison to pure ZnO. In 60 min, the optimized ZnO/AgKM reduced Cr(VI) by more than 98%, with a rate constant 63 times faster than that of pure ZnO. The enhancement of the separation and transportation of photogenerated electron-hole pairs, as proven by a decrease in photoluminescence intensity when compared with ZnO, was attributed to the composite's higher Cr(VI) reduction rate. Also, the formation of a new electronic level was created when AgKM are loaded on the surface of ZnO in the composites, as shown by the energy-resolved distribution of the electron trap (ERDT) pattern resulting to enhancement of light absorption ability by narrowing the energy band gap. Thus, ZnO/AgKM composite's photocatalytic efficacy was enhanced by its narrow energy band gap and reduced charge recombination. Therefore, the newly produced ZnO/AgKM composite can be used as a photocatalyst to purify Cr(VI)-containing wastewater.

Keywords: photocatalyst; Cr(VI) reduction; ZnO; AgNPs; cinnamon; wastewater treatment



Citation: Rizki, I.N.; Inoue, T.; Chuaicham, C.; Shenoy, S.; Srikaow, A.; Sekar, K.; Sasaki, K. Fabrication of Reduced Ag Nanoparticle Using Crude Extract of Cinnamon Decorated on ZnO as a Photocatalyst for Hexavalent Chromium Reduction. *Catalysts* **2023**, *13*, 265. <https://doi.org/10.3390/catal13020265>

Academic Editor: Didier Robert

Received: 5 December 2022

Revised: 16 January 2023

Accepted: 21 January 2023

Published: 24 January 2023



Copyright: © 2023 by the authors. Licensee MDPI, Basel, Switzerland. This article is an open access article distributed under the terms and conditions of the Creative Commons Attribution (CC BY) license (<https://creativecommons.org/licenses/by/4.0/>).

1. Introduction

For nanoparticle synthesis, either the top-down or bottom-up approach can be used. This includes chemical, physical, and biological approaches. In chemical processes, it is assumed that highly hazardous reagents, carcinogenic solvents, and environmental degradation are produced. On the other hand, some physical methods are energy-intensive and require costly equipment. In addition, both procedures resulted in challenges controlling crystal development and subsequently caused particle aggregation due to the necessity for extra stages involving the inclusion of a stabilizer. Through the production of metal nanoparticles from biological sources, nanobiotechnology offers enormous potential to promote eco-friendly systems and industrial sustainability [1]. For example, metallic nanoparticles such as silver (Ag), gold (Au), iron (Fe), selenium (Se), etc, have been synthesized using various biological agents [2–5]. This method is highly efficient and more environmentally friendly than conventional methods [6], cost-effective, does not require high pressure and temperature [7], and is without toxic chemicals [8].

Nowadays, silver (Ag) in the form of nanoparticles is more required in industrial process than in bulky form. In recent years, the manufacture of silver nanoparticles (AgNPs) has been developed using green chemical and biosynthetic methods involving

macro- (e.g., plants and its extracts) and microorganisms (bacteria, fungi, algae) as reducing agents [9].

Plant extracts are able to be utilized for biosynthesis of nanoparticles regarding their active compounds, i.e., sugars, green terpenoids, polyphenols, alkaloids, phenolic acids, and proteins, which used as capping, stabilizing, and reducing agents [10]. Owing to the abundance of tropical plants as well as possessing many biological activities such as antibacterial, antibiofilm, anthelmintic, anticancer, and antifungal activity [11–16], cinnamon (*Cinnamomum verum*) was used for the green synthesis of AgNPs. Cinnamon bark extract has been utilized widely for the synthesis of various metallic nanoparticles, such as Cu [17], Au [18], Ag [19], Se [20], as well as metal oxide nanoparticles, e.g., ZnO [21] and FeO [22]. A capping agent, cinnamic acid, is reported to be contained in cinnamon [23]. It has been revealed that the bioreduction of Ag^+ [24] and AuCl_4^- ions in cinnamon is mostly due to polyols such as terpenoids, flavones, and polysaccharides [25]. Other studies reported that the extract of *C. verum* contains around 80 aromatic components, such as saponins, terpenes, alkaloids, flavonol, tannin, cinnamyl aldehyde, corvalol, glycerol, and cinnamyl acetate, eugenol, etc [16,26].

Of the various applications of nanoparticles, especially precious metals, AgNPs have gained particular attention, and their use has been extensively investigated. AgNPs have good characteristics that can be utilized in various fields, mostly in the medical fields as antimicrobials [27–31], antiseptic [32], anticancer [8], as well as other industrial applications, including catalyst in chemical reactions, spectrally selective coatings for absorption of solar energy [33], food additives, textile industry [34], agriculture [35] and others.

Photocatalysis is a unique approach that is widely used and utilized in many various fields of study, including the removal of dangerous inorganic and organic pollutants from wastewater, the purification of contaminated air, the elimination of pesticides, and others [36–40]. Zinc oxide (ZnO) is prominent material in the field of photocatalysis for environmental management system. It has exclusive nature, e.g., direct and wide band gap in the near-UV spectral region, robust oxidation capability, good photocatalytic property, and a large free-exciton binding energy [41–45]. Nonetheless, this material has few shortcomings for the wide band gap energy and photocorrosion, resulting in low photocatalytic efficiency [46].

To enhance the activity as well as circumvent the electron-hole pair recombination, AgNPs can be synthesized as nanocomposite, i.e., zinc oxide (ZnO) [47]. One of the intriguing applications of AgNPs is an Ag/ZnO nanocomposite that can be used as an antimicrobial and anticancer [48] as well as increasing photocatalytic activity [22,49] and others.

Here, we investigate the ZnO-doped green reduced AgNPs using crude extract of cinnamon (AgKM) that were manufactured separate step. Multiple methods were employed to characterize the optical and physicochemical features of the produced products. Furthermore, ZnO's light-absorbing capacity was improved as a result of the production of heterojunction between ZnO and AgKM, which improved the separation of the e^- - h^+ pairs. The engineered materials showed remarkable charge transport characteristics and high photocatalytic activity for Cr(VI) degradation.

2. Results and Discussion

2.1. Phase Structure

The crystal phase structures of ZnO and ZnO/AgKM composites was determined using XRD analysis as are shown in Figure 1. In both the ZnO and ZnO/AgKM composites, distinct peaks were observed at 31.7° , 34.5° , and 36.3° , which correspond to the planes (100), (002), and (101) of the ZnO crystal phase, respectively (JCPDS No. 36-1451), indicating the successful hydrothermal production of ZnO. Due to the low concentration of Ag in the composites, the ZnO/AgKM composites exhibited no distinct peaks of Ag nanoparticles when AgKM solution was injected during composite synthesis. In

addition, a decrease in the (101) plane's peak intensity was found in the composite samples. This was attributable to the plan distortion by deposition of AgKM on the surface of ZnO. The crystallite size of ZnO and ZnO/AgKM composites was calculated based on XRD results. The crystallite size of ZnO, ZnO/AgKM-7 and ZnO/AgKM-10 was 583 Å, 560 Å and 575 Å, respectively. It can be seen that the introduction of AgNPs on the surface of ZnO in the composite samples showed the smaller crystallite size of ZnO, suggesting that the successful formation of heterojunction between ZnO and AgNPs via deposition of AgNPs. Also, the smaller crystallite size of the composites might provide larger surface area due to smaller particles, resulting in the enhancement of photocatalytic performance.

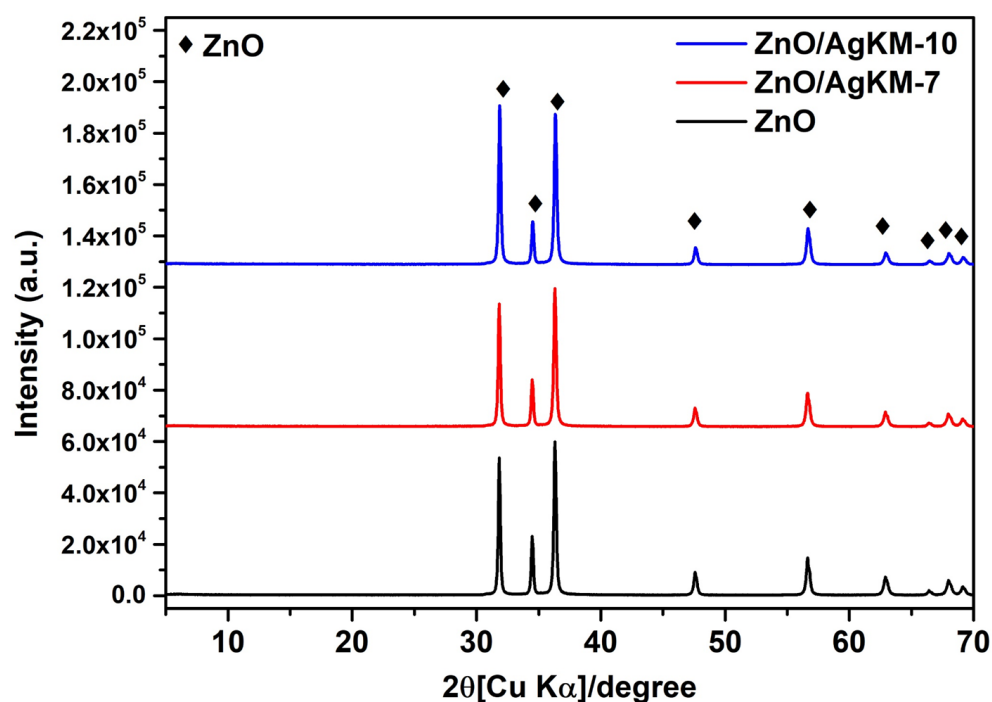


Figure 1. XRD patterns of ZnO, ZnO/AgKM-7 and ZnO/AgKM-10.

The composition of AgNPs in the composites was elucidated using XRF analysis. It was found that the ZnO/AgKM-7 contains AgNPs content around 3.38%wt while the ZnO/AgKM-10 has AgNPs about 3.26 %wt. Both of the composite samples showed a similar composition of AgNPs (around 3.3%), however the AgNPs content still low for detection by XRD analysis.

However, the presence of AgNP was confirmed by later analysis such as SEM-EDX, TEM-EDX, and XPS.

2.2. Optical Properties

Light absorption ability and energy bandgap (E_g) of photocatalyst are significant optical properties for the photocatalytic reaction. Thus, the ZnO and ZnO/AgKM composites were determined by UV-DRS technique to elucidate its optical properties. As depicted in Figure 2a, ZnO displayed robust light absorption in the wavelength range of 300–400 nm, indicating that it can be employed as a photocatalyst primarily in the UV light region. However, the ZnO/AgKM composites absorbed substantially more ultraviolet and visible light than ZnO (approximate wavelength range of 300–700 nm). This implied that the ZnO's optical characteristics were improved by the addition of AgKM. Thus, increasing the composite's light-harvesting capability can enhance its photocatalytic Cr(VI) reduction activity due to the large creation of charge carriers that participate in photocatalysis. Using Tauc's equation, the E_g values of ZnO and ZnO/AgKM composite samples were estimated.

As depicted in Figure 2b, calculated E_g values for ZnO, ZnO/AgKM-7, and ZnO/AgKM-10 are 3.16, 3.12 and 3.11 eV, respectively. All ZnO/AgKM composites had a lower E_g than pure ZnO, which may be attributable to the formation of a new electronic level due to a surface defect generated by AgKM. The decreasing E_g values of the composites may boost the generation of the e^- - h^+ pairs during light irradiation, hence enhancing the photocatalytic efficacy of the composites for Cr(VI) reduction. The incorporation of AgNP on the surface of the composite can slightly reduce the energy band gap of ZnO because AgNP did not alter the structure of ZnO, but rather deposited on the surface of ZnO to prevent the recombination of charge carriers.

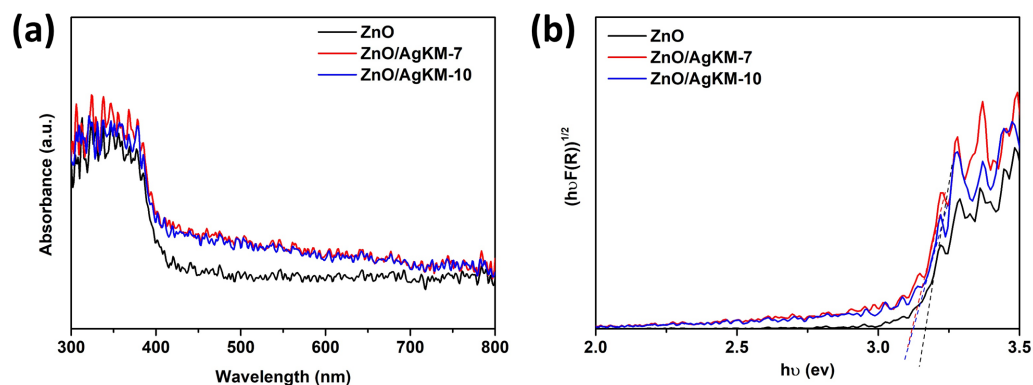


Figure 2. (a) UV-vis DRS spectra and (b) energy band gap plots of ZnO, ZnO/AgKM-7 and ZnO/AgKM-10.

In addition, reversed double-beam photoacoustic spectroscopy (RDB-PAS) was used to examine the surface electronic properties of ZnO, ZnO/AgKM-7, and ZnO/AgKM-10 (Figure 3). In order to elucidate the surface electronic characteristics of a photocatalyst in relation to its photocatalytic activity, the ERDT pattern obtained from RDB-PAS analysis of ZnO, ZnO/AgKM-7, and ZnO/AgKM-10 was plotted as a function of the energy from the valence band top (VBT) vs the electron trap density. It can be seen that ZnO displayed an electron accumulation density peak at roughly 3.0–3.2 eV, which was close to the bottom of the material's conduction band (CBB). The proximity of an electron trap state (ETs) to the CBB indicated that the synthesized ZnO photocatalyst possessed n-type semiconductor. However, the lower electron accumulation density of pure ZnO compared with TiO_2 and C_3N_4 [50–52] may be attributable to the fact that pure ZnO has fewer empty electron trap states and smaller ETs. Intriguingly, the ERDT pattern of the ZnO/AgKM composites showed a modest shift to a higher energy level at 3.0–3.2 eV, indicating that the introduction of the AgKM on the surface of ZnO damaged the crystallinity of the ZnO main structure in the composite, which is consistent with the decrease in XRD intensity. In addition, the composites exhibited a larger electron accumulation density than the pristine, indicating that the surface defect of ZnO caused by decorated AgKM might generate additional electron trap states, resulting in a decrease in E_g of the composite. Moreover, it is probable that the electron in the electron trap states migrated to the AgKM, concurrently generating empty electron trap states to accept electrons during measurement. Also, the electron transport from ZnO to AgKM via the heterojunction effect between ZnO and AgKM could prevent the recombination of photogenerated electron-hole pairs.

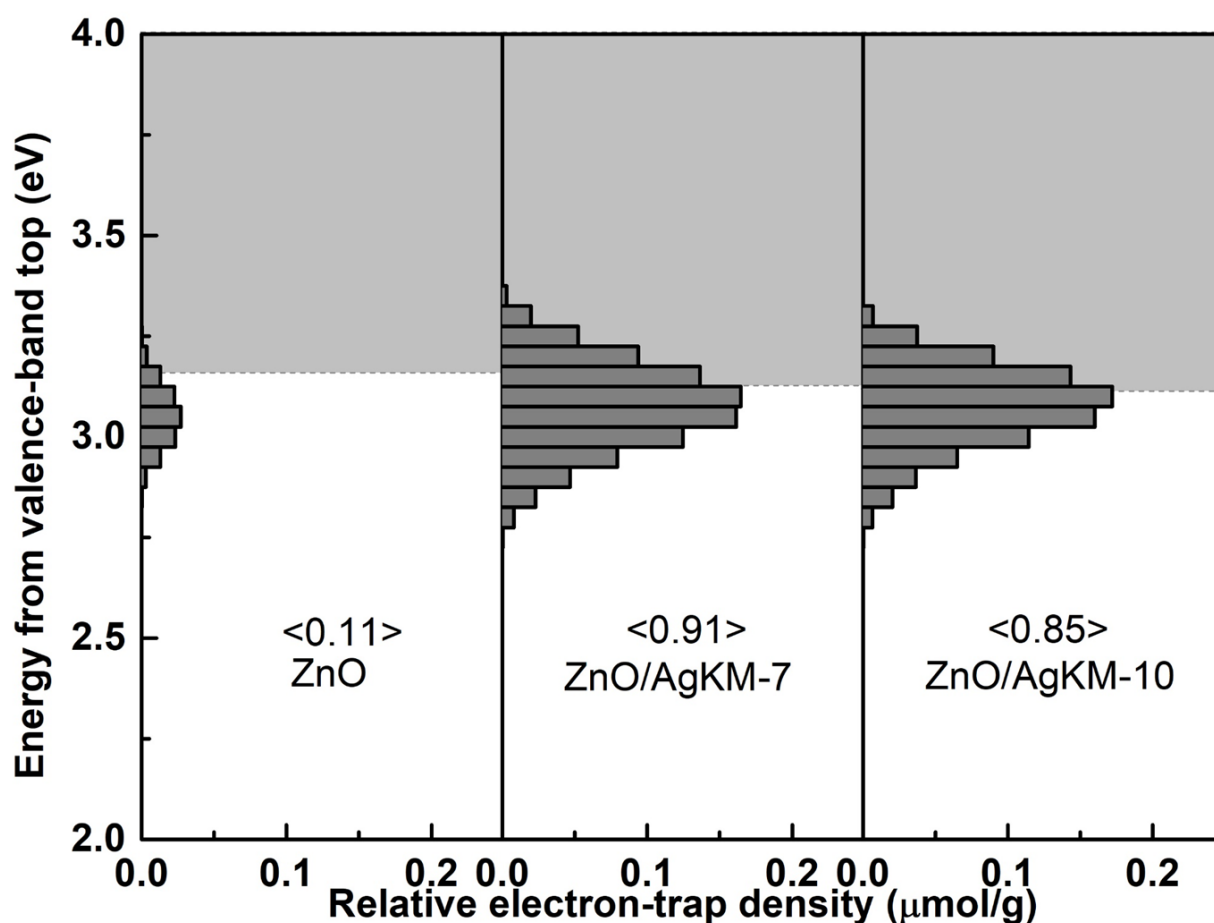


Figure 3. ERDT/ CBB patterns including relative total electron trap density in brackets of ZnO, ZnO/AgKM-7 and ZnO/AgKM-10.

2.3. Morphology Results

Figure 4 depicts the SEM-detected surface morphologies of ZnO, ZnO/AgKM-7, and ZnO/AgKM-10. In the case of pure ZnO (Figure 4a,b), the surface morphology revealed agglomerates of microscopic ZnO particles forming a flower-like structure with widths of around 3–4 μm . Intriguingly, the ZnO/AgKM composites displayed rod-like morphology which is piece of ZnO flower-like structure with smaller particle sizes than pure ZnO (Figure 4c–f), indicating that the inclusion of AgKM solution influenced the crystallization of ZnO particles. In addition, the smaller size of ZnO/AgKM composites may have a higher surface activity than that of pure ZnO, hence providing a larger surface active for photocatalytic Cr(VI) reduction. Also, ZnO, ZnO/AgKM-7, and ZnO/AgKM-10 had their elemental distributions clarified by scanning electron microscopy with energy dispersive X-ray spectroscopy (SEM-EDX). SEM-EDX was used to confirm the presence of AgNPs in the ZnO/AgKM composites, despite the fact that there appears to be no difference. In addition, the signal of Ag can be observed in the composite and the location of Ag signal overlapped with Zn and O signals implying that AgNPs might present on the surface of ZnO (Figure 4g–i).

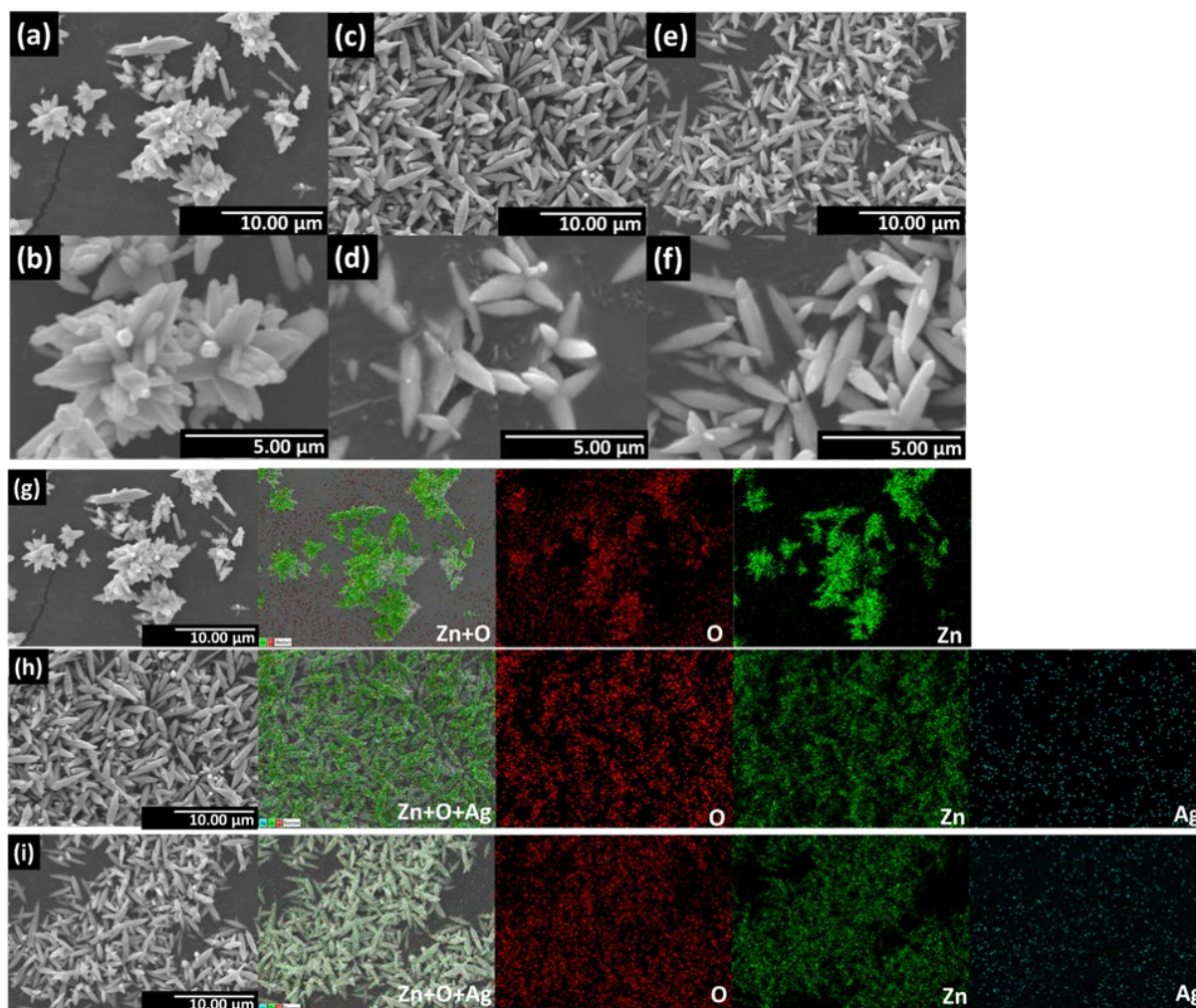


Figure 4. SEM images of (a,b) ZnO, (c,d) ZnO/AgKM-7, and (e,f) ZnO/AgKM-10 with different magnifications, and SEM-EDX images of (g) ZnO, (h) ZnO/AgKM-7, and (i) ZnO/AgKM-10.

Additionally, TEM-mapping investigation verified the existence of AgKM on the surface of ZnO. As depicted in Figure 5(a,b), TEM investigation validated the morphology and particle size of produced AgKM. It can be noted that the well-distribution of small spherical particles was found under both synthetic circumstances (pH 7 and pH 10), indicating that the use of an organic extract from cinnamon could reduce Ag^+ ions to AgKM and prevent their agglomeration. The particle size distribution of AgKM was analyzed and depicted in Figure 5c. It is evident that the smaller size of AgKM obtained at pH 7 corresponds to a larger contact area between ZnO and AgKM and a greater production of new electronic states by surface distortion of ZnO utilizing AgKM in the ZnO/AgKM-7. Moreover, the high magnification TEM image of ZnO/AgKM-7 unveils the dark spot on the surface of ZnO in the bright field image and brilliant spot on the surface of ZnO in the dark field image, which may indicate the existence of heavily Ag NPs on the surface of ZnO (Figure 5(d-g)). Moreover, TEM-EDX mapping of the ZnO/AgKM composites revealed the deposition of AgKM on the ZnO surface in the composites. The ZnO/AgKM composites exhibited significant Zn and O signals in their mapping, indicating that they were the primary constituents of ZnO, while the signals of Ag as minor components were located in the same area as the dark spot in the bright field TEM image, confirming the deposition of AgKM in the composite (Figure 5h).

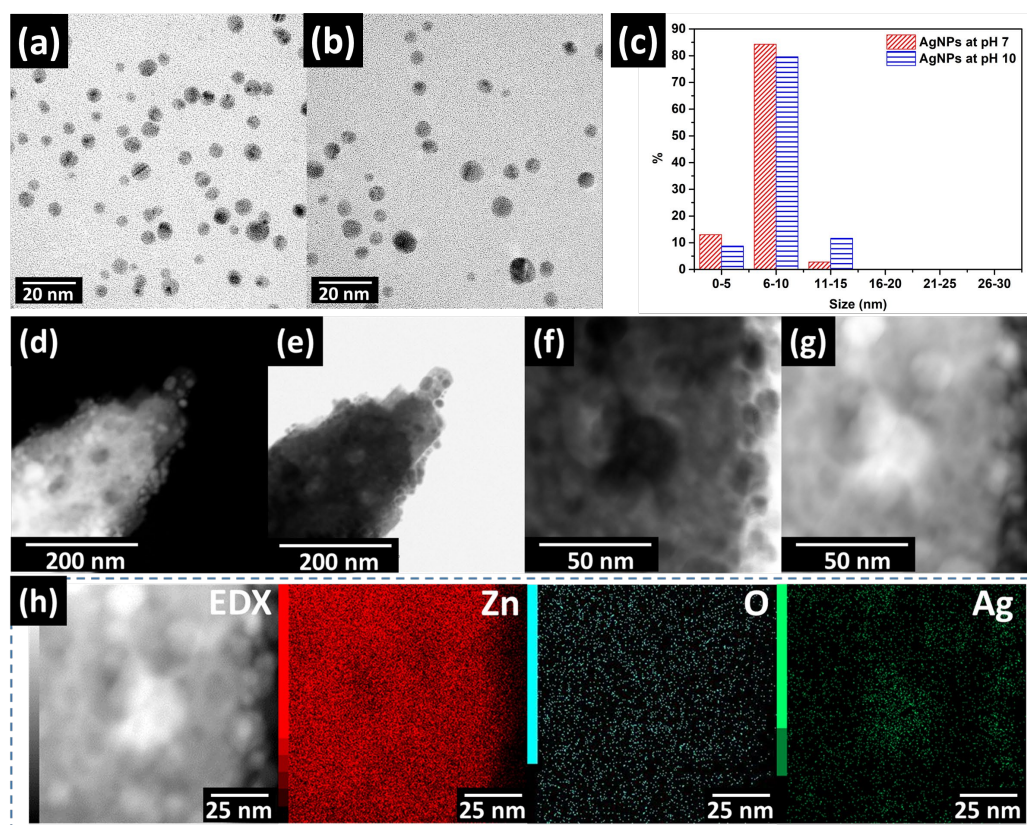


Figure 5. TEM images of (a) AgKM produced at pH 7, (b) AgKM produced at pH 10, (c) particle size distribution of AgKM, (d,f) bright field images of ZnO/AgKM-7 and (e,g) dark field images of ZnO/AgKM-10. TEM-EDX images of (h) ZnO/AgKM-10.

2.4. Chemical State and Band Positions

The chemical states of Zn, O, and Ag, as well as the VB position of ZnO and the optimized ZnO/AgKM-7 composite were investigated by XPS analysis. Examining the spectra of ZnO and ZnO/AgKM-7 composites revealed that the synthesized samples primarily consist of Zn and O. Due to low addition content, the Ag signal was not clearly noticed in survey scans (Figure 6a). The Zn 2p spectrum of ZnO and ZnO/AgKM-7 composite for narrow scan is depicted in Figure 6b, where two peaks correspond to the Zn 2p orbitals of ZnO and ZnO/AgKM-7 composite. Zn 2p_{3/2} orbital may account for the strongest signal at 1021 eV, whereas Zn 2p_{1/2} orbital is accountable for the remaining peak at 1045 eV. These two peaks' binding energy corroborated the divalent status of the Zn ion in the ZnO structure. Moreover, Figure 6c depicts the O 1s spectra of ZnO and ZnO/AgKM-7 composite, which exhibit three distinct component peaks at 530.2, 531.1, and 532.3 eV, corresponding to the Zn-O bond, Zn-OH, and adsorbed H₂O, respectively. Moreover, as shown by the spectra of the Ag 3d orbitals in Figure 6d, the two principal peaks at EB [Ag 3d_{5/2}] was observed at 367.2 eV and 368.6 eV in the ZnO/AgKM-7 composite due to the Ag-O and decorated Ag(0) of AgKM present in the composite. Using XPS, the valence regions of ZnO and the ZnO/AgKM-7 composite were analyzed. As shown in Figure 6e, the predicted VB position of ZnO and ZnO/AgKM-7 are 2.5, 1.75, and 1.39 eV, respectively. In Figure 6f, the CB locations of ZnO and ZnO/AgKM-7 composite were calculated to be −0.66, −1.37 and −1.72 eV, respectively, using UV-DRS data.

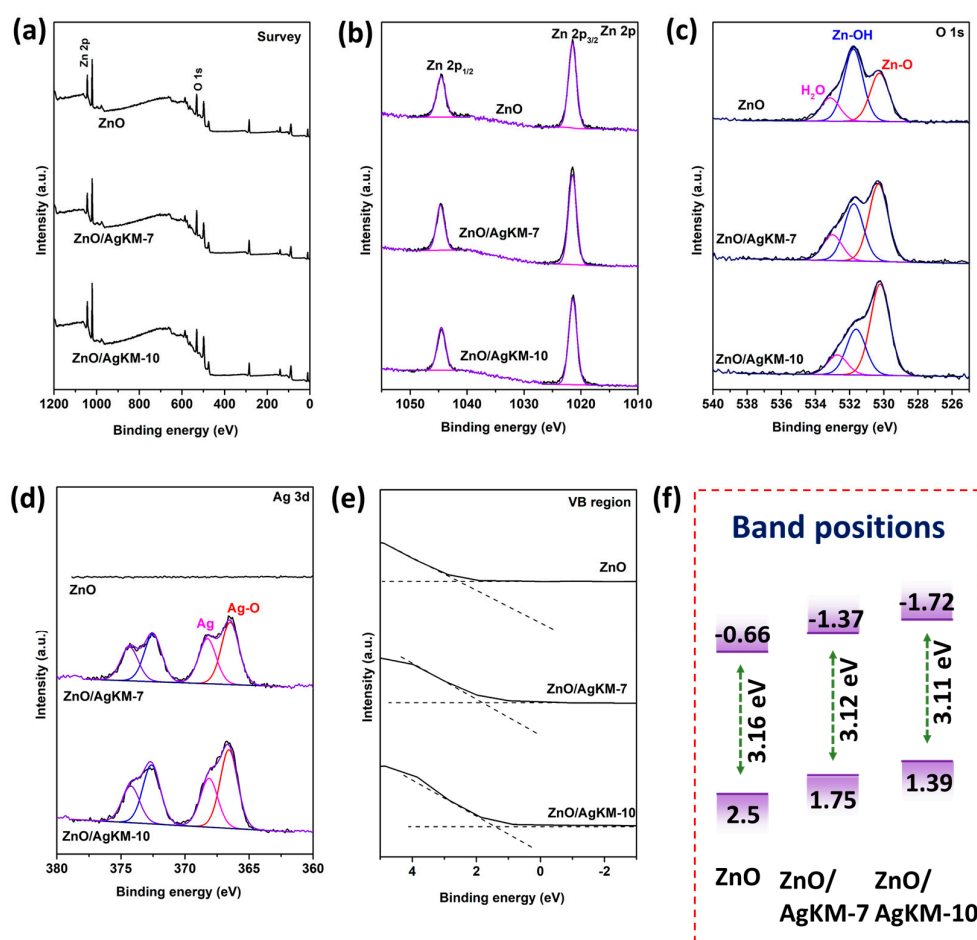


Figure 6. XPS spectra of ZnO, ZnO/AgKM-7, and ZnO/AgKM-10: (a) survey spectra, (b) Zn 2p, (c) O 1s, (d) Ag 3d, (e) valence band energy region, and (f) band position.

2.5. Photocatalytic Cr(VI) Reduction

Under visible light irradiation, the photocatalytic activities of ZnO, ZnO/AgKM-7, and ZnO/AgKM-10 were determined by measuring the reduction of Cr(VI). In the photocatalytic reaction, the Cr(VI) was reduced by the electron which was produced from photocatalyst under irradiation. Also in the reaction ethanol was utilized as a hole scavenger to prevent re-oxidation of Cr(III).

In Figure 7a, under dark conditions, ZnO exhibited less Cr adsorption (about 1%) than the ZnO/AgKM-7 and ZnO/AgKM-10 composites, which had roughly 10% greater Cr(VI) adsorption capacity than pure ZnO. This could be a result of the increased electrostatic interactions between the surface active of ZnO/AgKM composites and Cr(VI) ions. To assess their photocatalytic activity under UV-visible light irradiation, the reduction efficiencies (C/C_0) of Cr(VI) were determined for each sample. Basically, the adsorption of Cr(VI) under dark condition before catalytic reaction was conducted in order to prove the removal of Cr(VI) between adsorption and photocatalytic reaction. It is clear that in the dark condition, the concentration of Cr(VI) was reduced less than 10%. However, after irradiation, the concentration of Cr(VI) dramatically decrease proving that the main removal process of Cr(VI) is photocatalytic reaction. In detail, under the dark condition, the composite showed higher adsorption ability of Cr(VI) because the deposited AgNPs on the surface of ZnO reduced the particle size of ZnO confirmed by SEM image, resulting in providing larger active surface site for adsorption and photocatalytic reaction. In addition, C/C_0 is the ratio between the concentration of Cr(VI) after treatment over the initial concentration of Cr(VI).

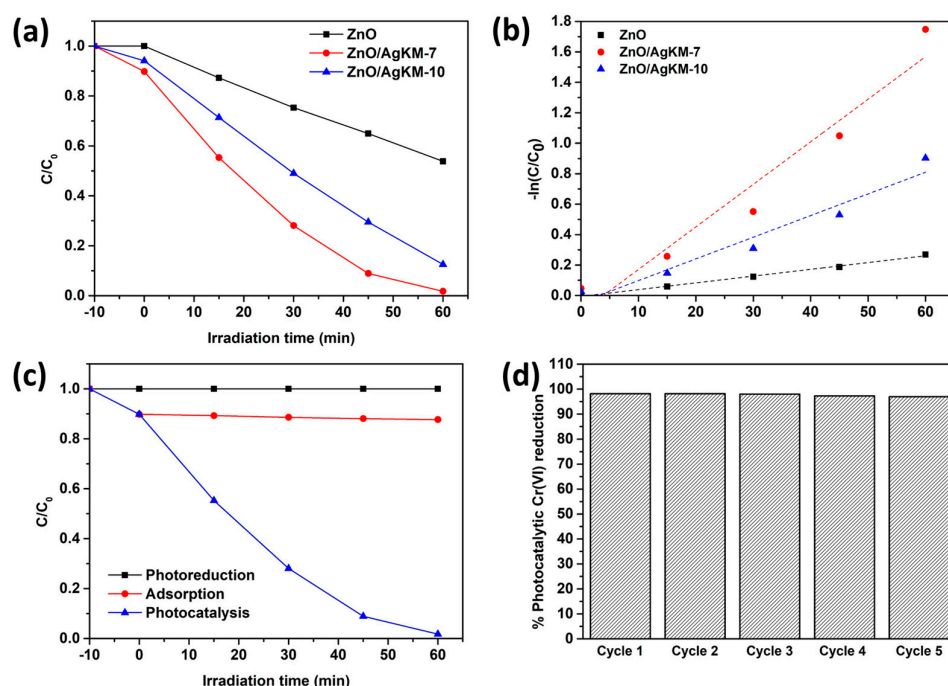


Figure 7. (a) Time course and (b) pseudo-first-order kinetics plots of photocatalytic Cr(VI) conversion over ZnO, ZnO/AgKM-7 and ZnO/AgKM-10, (c) photo-reduction and adsorption test using ZnO/AgKM-7, (d) Photocatalytic Cr(VI) conversion over five cycles using ZnO/AgKM-7.

For Cr(VI) reduction, the photogenerated electron can react with Cr(VI) and reduced them to Cr(III) simultaneously the photogenerated hole was consumed by ethanol as a hole scavenger. After 60 min of reaction, the C/C_0 values of ZnO, ZnO/AgKM-7, and ZnO/AgKM-10 were 0.54, 0.0178 and 0.125, respectively. Both ZnO/AgKM-7 and ZnO/AgKM-10 displayed photocatalytic Cr(VI) reduction activity (98%) within 60 min, demonstrating its suitability for Cr(VI) reduction. ZnO/AgKM composites exhibited greater photocatalytic Cr(VI) reduction activities than pure ZnO, as evidenced by the development of a novel electron trap state that decreased the energy bandgap. As shown in Figure 7b, the photocatalytic Cr(VI) reduction rates of ZnO, ZnO/AgKM-7, and ZnO/AgKM-10 were fitted using a pseudo-first-order kinetic model [53]. ZnO, ZnO/AgKM-7, and ZnO/AgKM-10 had reaction rate constants (k) of 0.0044, 0.0279 and 0.0143 min^{-1} , respectively. ZnO/AgKM-7 had the greatest rate constant, with a value that was 63 times that of pure ZnO. The photo-reduction under light irradiation without the inclusion of the ZnO/AgKM-7 and the adsorption test under dark conditions utilizing the ZnO/AgKM-7 confirmed the removal process of Cr(VI), as shown in Figure 5c. It is evident that photo-reduction was unable to decrease the Cr(VI) concentration, while the adsorption-desorption equilibrium of Cr(VI) on the surface of the composite was obtained in less than 10% within 10 min and it stayed constant after the equilibrium was attained. In contrast, the photocatalytic process demonstrated a substantial decrease in Cr(VI) content after 60 min, indicating that photocatalysis is the major mechanism for reducing Cr(VI) (Figure 7c). Thus, these results reveal that decorating the surface of ZnO with decreased AgKM using cinnamon can dramatically promote the composite's photocatalytic Cr(VI) reduction activity. The recycling test reusability was conducted using the spent photocatalyst from the previous cycle without any treatment (Figure 7d).

2.6. ZnO/AgKM-7 Stability

The stability and reusability of catalysts are critical to their practical application. Using five cycles of ZnO/AgKM-7 for Cr(VI) reduction, the product's recyclability was examined. As depicted in Figure 7d, the photocatalytic Cr(VI) reduction over ZnO/AgKM-7 was maintained over five cycles with a remarkable removal percentage of over 96%, suggesting

that ZnO/AgKM-7 has good stability and recyclability for photocatalytic Cr(VI) reduction under light irradiation. After the initial photocatalytic Cr(VI) reduction, the phase structure of ZnO/AgKM-7 after the first cycle was analyzed using XRD in order to compare its stability to that of fresh ZnO/AgKM-7. Comparing the two diffraction patterns reveals that the Cr(VI) reduction had no effect on the ZnO/AgKM-7 phase structures, as depicted in Figure 8a, demonstrating that ZnO/AgKM-7 is highly stable for Cr(VI) reduction.

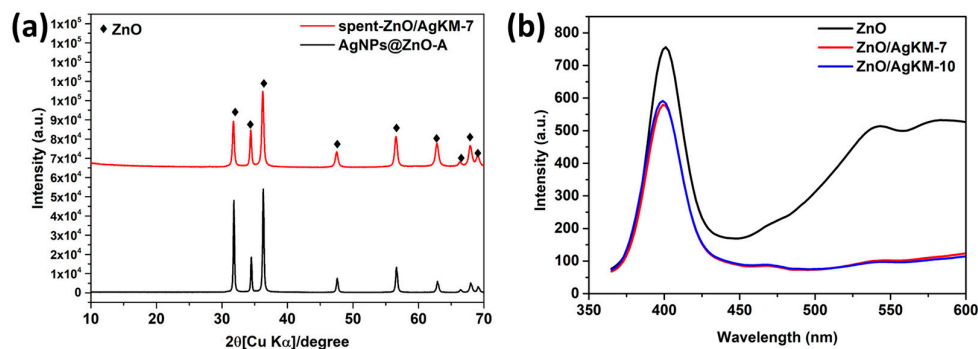


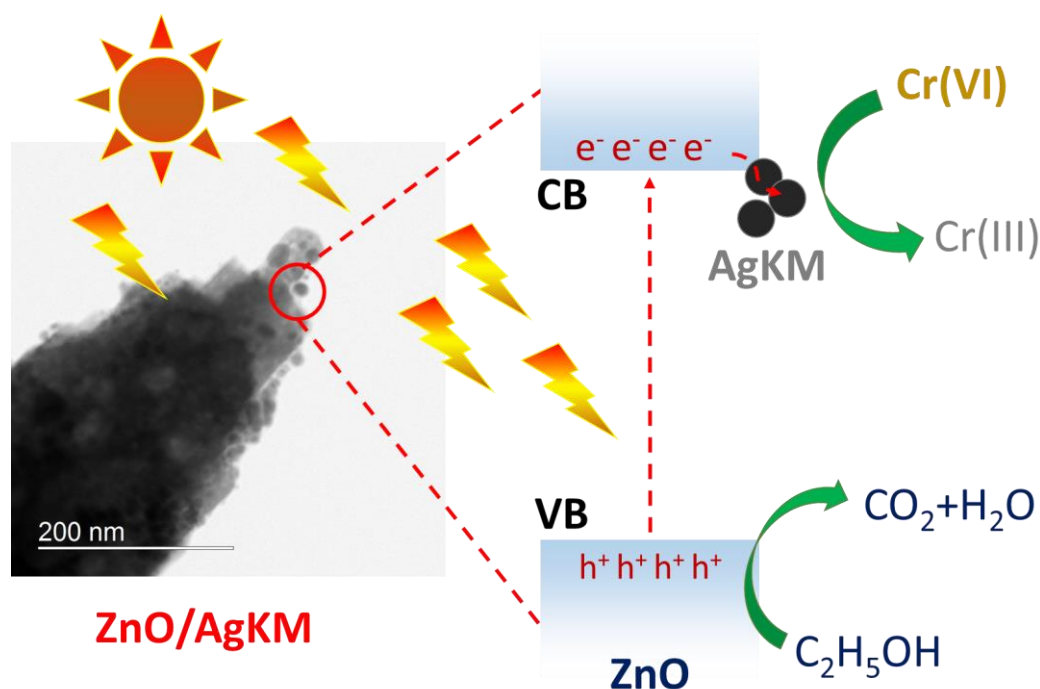
Figure 8. (a) XRD patterns of fresh ZnO/AgKM-7 and spent ZnO/AgKM-7, and (b) PL spectra of ZnO, ZnO/AgKM-7, and ZnO/AgKM-10.

2.7. Examination of the Transfer and Separation of Charges

The effect of heterojunction between ZnO and AgKM in the composite and the development of a new electron trap state by AgKM deposition on the surface of ZnO on the separation and transfer of $e^- - h^+$ pairs was investigated using PL analysis. The ZnO/AgKM-7 composite with the highest photocatalytic performance was chosen for comparison with the pure ZnO photocatalyst. As depicted in Figure 8b, the ZnO and ZnO/AgKM-7 emission spectra are in the 365–600 nm area. In general, a low PL intensity indicates a low rate of $e^- - h^+$ pair recombination. The heterojunction between ZnO and AgKM in the composite and development of new electron trap state in the ZnO/AgKM-7 improved the charge carrier separation, as demonstrated by the lowered PL emission intensity of ZnO/AgKM-7 relative to ZnO at about 400 nm for a 350 nm excitation wavelength. The development of the heterojunction between ZnO and AgKM in the composite and the formation of a novel electron trap state in the ZnO/AgKM-7 sample improved the electronic features, including charge separation and electron transport, as determined by the PL data. Moreover, through the TEM images (Figure 5), the deposition of AgNPs on the ZnO confirming that the surface heterojunction was formed in the composite.

2.8. Photocatalytic Mechanism

Scheme 1 illustrates a proposed photocatalytic Cr(VI) reduction process employing ZnO/AgKM-7 composite based on the outcomes of this work. The VB and CB of the composite ZnO/AgKM-7 were 1.75 and -1.37 eV, respectively. Under the influence of light, the ZnO/AgKM-7 composite produced $e^- - h^+$ pairs. The excited electrons migrated from the VB to a new electronic state formed by the defect in the ZnO structure and CB of ZnO, while concurrently producing holes in the VB. Then, the excited electron from ZnO can be segregated by migrating to the surface of AgKM via heterojunction to prevent the recombination of $e^- - h^+$ pairs, thereby enhancing the photocatalytic activity of ZnO/AgKM-7. Through the photocatalytic reaction, the accumulated electrons on the surface of AgKM can reduce Cr(VI) to Cr(III). Additionally, ethanol consumed h^+ in the VB of ZnO/AgKM-7 via oxidation process to avoid the re-oxidation of Cr(III). The formation of a heterojunction with ZnO/AgKM-7 increased the amount of active electrons responsible for the photocatalytic reduction of Cr(VI). In the absence of light, there is no photocatalytic activity since the catalyst is incapable of producing electrons for Cr(VI) reduction. Consequently, only adsorption may occur in a dark environment.



Scheme 1. Photocatalytic degradation mechanism of Cr reduction over ZnO/AgKM composite.

3. Materials and Methods

3.1. Chemicals

Fujifilm Wako Pure Chemical Co. (Osaka, Japan) provided the following for the synthesis and all experiments: Ammonium hydroxide (NH₄OH, 28%wt NH₄OH in water), zinc nitrate hexahydrate (Zn(NO₃)₂•6H₂O), sodium chromate tetrahydrate (Na₂CrO₄•4H₂O), silver nitrate (AgNO₃) and water. All of the chemicals used were of pure analytical grade and required no further purification. Ultrapure water was used in the experiments with the organic color solutions.

3.2. Preparation of the Plant Extract

An effective reducing agent for the synthesis of silver nanoparticles (AgKM) was cinnamon (*Cinnamomum verum*). The cinnamon bark was oven-dried at 80 °C for 12 h prior to grinding into a powder. The crude plant extract was prepared by boiling 10% *w/v* of plant powder with distilled water in a beaker glass for 10 min. The solution was allowed to cool to room temperature, then filtered using a Whatman no. 41 [54] filter. The unfiltered concentrate was put to use in subsequent testing.

3.3. Synthesis Silver Nanoparticles Using Crude Extract of Cinnamon (AgKM)

The formation of AgKM is reliant on a number of factors. The precursor used to create the AgKM was silver nitrate (AgNO₃). A value of 2 mM was chosen as the concentration. The dilution rate of the crude extract applied to the Ag solution was 1% *v/v*. NaOH was used to bring the solution's pH to 7 and 10. The solutions were shaken for 2 h at 30 °C and 200 rpm in an incubator. At the end of the incubation period, samples were taken out and analyzed to determine the particle size distribution.

3.4. ZnO and ZnO/AgKM Synthesis

Hydrothermal synthesis was used to create ZnO/AgKM composites. This was accomplished by adding 2.975 g of Zn(NO₃)₂•6H₂O, 2.8 mL of 28%wt NH₄OH in water, and a certain amount of AgKM solution (46.4 mmol) to a 100 ml Teflon autoclave, bringing the entire volume up to 50 mL with DI water, sealing the container, and heating it at 160 °C for 24 h. The resulting solid product was then filtered and washed multiple times with DI

water and ethanol. In addition, the obtained solid products were dried at 75 °C for 24 h. The composites were denoted as ZnO/AgKM-7 and ZnO/AgKM-10 when the composites were prepared by extracting AgKM from solutions at pH 7 and pH 10, respectively. Additionally, pure ZnO was made in a similar fashion, minus the inclusion of AgKM solution.

3.5. Characterization

The crystal phase structures of all materials were determined using an Ultima IV X-ray diffraction (XRD) apparatus (RIGAKU, Akishima, Japan). The morphology and surface parameters of all samples were confirmed using scanning electron microscopy (SEM, VE-9800, Keyence, Osaka, Japan). Using JEM-2100HCKM (JEOL Ltd., Tokyo, Japan), TEM pictures and TEM-EDX mapping were also observed. UV-Vis diffuse reflectance spectroscopy (UV-DRS, UV-2450 Shimadzu, Kyoto, Japan) was utilized to determine the light absorption capacities of pure and composite samples. The VB sites of all samples were determined by X-ray photoelectron spectroscopy (XPS, ESCA 5800; ULVAC-PHI, Inc., Kanagawa, Japan). Photoluminescence (PL) spectroscopic measurements were performed utilizing an FP-6600 spectrofluorometer (JASCO Corporation, Tokyo, Japan, FP-6600 spectrofluorometer). Reversed double-beam photoacoustic spectroscopy (RDB-PAS) from 650 to 300 nm using an amplifier to double the photoacoustic signals revealed the energy-resolved distribution of electron trap (ERDT) patterns of the manufactured materials.

3.6. Photocatalytic Cr(VI) Reduction

Experiments were carried out to determine the efficacy of photocatalytic activity in the reduction of Cr(VI). About 50 mg of fabricated composites are typically mixed with 50 mL of 10 ppm Cr(VI) aqueous solution in the dark for 30 min until adsorption-desorption equilibrium is attained. Prior to the photocatalytic process, 0.5 M HCl and 0.5 M NaOH were added to the suspension solutions to adjust the pH to 3. A 500 W Xe lamp was then utilized to illuminate the suspensions. To recover the resultant composites, the suspensions were withdrawn and filtered through 0.45 m membrane filters while the light was on. The remaining Cr(VI) concentration were determined using diphenyl carbazide colorimetric analysis with a UV-Vis spectrometer set to 554 nm.

4. Conclusions

Utilizing cinnamon bark extract to reduce Ag⁺ ions lead to a stable and smaller size of AgKM (average 6–10 nm). ZnO/AgKM composites were effectively produced by hydrothermally treating ZnO precursors in the presence of AgKM solution. ZnO/AgKM-7 revealed a reaction rate constant 63 times greater than that of pure ZnO, resulting in a high rate reduction of Cr(VI) degradation. In addition, ZnO/AgKM-7 exhibited the greatest photocatalytic Cr(VI) reduction compared to all other samples. This may be owing to the smaller particle size of the composite, which can provide a more active surface and a lower recombination rate for charge carriers. PL results indicated that development of heterojunction between AgKM and ZnO in the ZnO/AgKM composite inhibited electron-hole pair recombination. In addition, increased light absorption was accomplished by decreasing the energy band gap, which was made feasible by loading AgKM onto the surface of ZnO in the composites, as confirmed by ERDT data. The combination of a low energy band gap and reduced charge recombination increased the photocatalytic efficiency of the ZnO/AgKM composite. This study proposes an alternative ZnO/AgKM photocatalyst for the efficient treatment of wastewater including inorganic contaminants.

Author Contributions: I.N.R., C.C.: Conceptualization, Investigation, Writing—original draft, Writing—review & editing. T.I., K.S. (Karthikeyan Sekar), S.S., A.S., C.C.: Formal analysis. K.S. (Keiko Sasaki), C.C.: Conception, interpretation, editing the manuscript. All authors have read and agreed to the published version of the manuscript.

Funding: The work was supported by the Japan Society for the Promotion of Science (JSPS) KAKENHI (A) [No. JSPS JP22H00266]. This work was partly supported by Advanced Research Infrastructure for Materials and Nanotechnology Grant Number JPMXP1222KU1009 in Japan sponsored by the Ministry of Education, Culture, Sports, Science and Technology (MEXT), Japan. This work was partly supported by 2022 Research Start Program 202208 to Chitiphon Chuaicham. This work was partly supported by Hibah Riset Mandat Universitas Airlangga Indonesia No: 391/UN3.14/PT/2020.

Conflicts of Interest: There are no conflict of interest to declare by the authors.

References

1. Rizki, I.N.; Klaypradit, W. Utilization of marine organisms for the green synthesis of silver and gold nanoparticles and their applications: A review. *Sustain. Chem. Pharm.* **2023**, *31*, 100888. [\[CrossRef\]](#)
2. Fouda, A.; Hassan, S.E.-D.; Eid, A.M.; Abdel-Rahman, M.A.; Hamza, M.F. Light enhanced the antimicrobial, anticancer, and catalytic activities of selenium nanoparticles fabricated by endophytic fungal strain, *Penicillium crustosum* EP-1. *Sci. Rep.* **2022**, *12*, 11834. [\[CrossRef\]](#) [\[PubMed\]](#)
3. Roy, A.; Pandit, C.; Gacem, A.; Alqahtani, M.S.; Bilal, M.; Islam, S.; Hossain, M.; Jameel, M. Biologically derived gold nanoparticles and their applications. *Bioinorg. Chem. Appl.* **2022**, *2022*, 8184217. [\[CrossRef\]](#) [\[PubMed\]](#)
4. Mustapha, T.; Misni, N.; Ithnin, N.R.; Daskum, A.M.; Unyah, N.Z. A Review on Plants and Microorganisms Mediated Synthesis of Silver Nanoparticles, Role of Plants Metabolites and Applications. *Int. J. Environ. Res. Public Health* **2022**, *19*, 674. [\[CrossRef\]](#)
5. Ettadili, F.; Aghris, S.; Laghrib, F.; Farahi, A.; Saqrane, S.; Bakasse, M.; Lahrich, S.; El Mhammedi, M. Recent advances in the nanoparticles synthesis using plant extract: Applications and future recommendations. *J. Mol. Struct.* **2022**, *1248*, 131538. [\[CrossRef\]](#)
6. Anjum, S.; Khan, A.K.; Qamar, A.; Fatima, N.; Drouet, S.; Renouard, S.; Blondeau, J.P.; Abbasi, B.H.; Hano, C. Light Tailoring: Impact of UV-C Irradiation on Biosynthesis, Physiognomies, and Clinical Activities of *Morus macroura*-Mediated Monometallic (Ag and ZnO) and Bimetallic (Ag-ZnO) Nanoparticles. *Int. J. Mol. Sci.* **2021**, *22*, 11294. [\[CrossRef\]](#)
7. Hekmati, M.; Hasanirad, S.; Khaledi, A.; Esmaeili, D. Green synthesis of silver nanoparticles using extracts of *Allium rotundum* L, *Falcaria vulgaris* Bernh, and *Ferulago angulate* Boiss, and their antimicrobial effects in vitro. *Gene Rep.* **2020**, *19*, 100589. [\[CrossRef\]](#)
8. Singh, J.; Singh, T.; Rawat, M. Green synthesis of silver nanoparticles via various plant extracts for anti-cancer applications. *Nanomedicine* **2017**, *7*, 1–4.
9. Yousaf, H.; Mehmood, A.; Ahmad, K.S.; Raffi, M. Green synthesis of silver nanoparticles and their applications as an alternative antibacterial and antioxidant agents. *Mater. Sci. Eng. C* **2020**, *112*, 110901. [\[CrossRef\]](#)
10. Nadaroglu, H.; GÜNGÖR, A.A.; Selvi, İ. Synthesis of nanoparticles by green synthesis method. *Int. J. Innov. Res. Rev.* **2017**, *1*, 6–9.
11. Ahmad, M.; Lim, C.P.; Akowuah, G.A.; Ismail, N.N.; Hashim, M.A.; Hor, S.Y.; Ang, L.F.; Yam, M.F. Safety assessment of standardised methanol extract of *Cinnamomum burmannii*. *Phytomedicine* **2013**, *20*, 1124–1130. [\[CrossRef\]](#)
12. Kot, B.; Wicha, J.; Piechota, M.; Wolska, K.; Gruzewska, A. Antibiofilm activity of trans-cinnamaldehyde, p-coumaric, and ferulic acids on uropathogenic *Escherichia coli*. *Turk. J. Med. Sci.* **2015**, *45*, 919–924. [\[CrossRef\]](#)
13. Williams, A.R.; Ramsay, A.; Hansen, T.V.; Ropiak, H.M.; Mejer, H.; Nejsun, P.; Mueller-Harvey, I.; Thamsborg, S.M. Anthelmintic activity of trans-cinnamaldehyde and A-and B-type proanthocyanidins derived from cinnamon (*Cinnamomum verum*). *Sci. Rep.* **2015**, *5*, 14791. [\[CrossRef\]](#)
14. Zhang, J.-H.; Liu, L.-Q.; He, Y.-L.; Kong, W.-J.; Huang, S.-A. Cytotoxic effect of trans-cinnamaldehyde on human leukemia K562 cells. *Acta Pharmacol. Sin.* **2010**, *31*, 861–866. [\[CrossRef\]](#)
15. Bang, K.-H.; Lee, D.-W.; Park, H.-M.; Rhee, Y.-H. Inhibition of fungal cell wall synthesizing enzymes by trans-cinnamaldehyde. *Biosci. Biotechnol. Biochem.* **2000**, *64*, 1061–1063. [\[CrossRef\]](#)
16. Ansari, M.A.; Murali, M.; Prasad, D.; Alzohairy, M.A.; Almatroudi, A.; Alomary, M.N.; Udayashankar, A.C.; Singh, S.B.; Asiri, S.M.M.; Ashwini, B.S. *Cinnamomum verum* bark extract mediated green synthesis of ZnO nanoparticles and their antibacterial potentiality. *Biomolecules* **2020**, *10*, 336. [\[CrossRef\]](#)
17. Sarwar, N.; Humayoun, U.B.; Kumar, M.; Zaidi, S.F.A.; Yoo, J.H.; Ali, N.; Jeong, D.I.; Lee, J.H.; Yoon, D.H. Citric acid mediated green synthesis of copper nanoparticles using cinnamon bark extract and its multifaceted applications. *J. Clean. Prod.* **2021**, *292*, 125974. [\[CrossRef\]](#)
18. ElMitwalli, O.S.; Barakat, O.A.; Daoud, R.M.; Akhtar, S.; Henari, F.Z. Green synthesis of gold nanoparticles using cinnamon bark extract, characterization, and fluorescence activity in Au/eosin Y assemblies. *J. Nanoparticle Res.* **2020**, *22*, 309. [\[CrossRef\]](#)
19. Anjum, S.; Jacob, G.; Gupta, B. Investigation of the herbal synthesis of silver nanoparticles using *Cinnamon zeylanicum* extract. *Emergent Mater.* **2019**, *2*, 113–122. [\[CrossRef\]](#)
20. Alghuthaymi, M.A.; Diab, A.M.; Elzahy, A.F.; Mazrou, K.E.; Tayel, A.A.; Moussa, S.H. Green biosynthesized selenium nanoparticles by cinnamon extract and their antimicrobial activity and application as edible coatings with nano-chitosan. *J. Food Qual.* **2021**, *2021*, 6670709. [\[CrossRef\]](#)

21. Mohapatra, S.; Leelavathi, L.; Meignana, A.I.; Pradeep, K.R.; Rajeshkumar, S. Assessment of Antimicrobial Efficacy of Zinc Oxide Nanoparticles Synthesized Using Clove and Cinnamon Formulation against Oral Pathogens—An In Vitro Study. *J. Evol. Med. Dent. Sci.* **2020**, *9*, 2034–2040. [[CrossRef](#)]
22. Ahmad, W.; Kumar Jaiswal, K.; Amjad, M. Euphorbia herita leaf extract as a reducing agent in a facile green synthesis of iron oxide nanoparticles and antimicrobial activity evaluation. *Inorg. Nano-Met. Chem.* **2021**, *51*, 1147–1154. [[CrossRef](#)]
23. Nabi, G.; Raza, W.; Tahir, M. Green synthesis of TiO₂ nanoparticle using cinnamon powder extract and the study of optical properties. *J. Inorg. Organomet. Polym. Mater.* **2020**, *30*, 1425–1429. [[CrossRef](#)]
24. Saqib, S.; Faryad, S.; Afridi, M.I.; Arshad, B.; Younas, M.; Naeem, M.; Zaman, W.; Ullah, F.; Nisar, M.; Ali, S. Bimetallic assembled silver nanoparticles impregnated in aspergillus fumigatus extract damage the bacterial membrane surface and release cellular contents. *Coatings* **2022**, *12*, 1505. [[CrossRef](#)]
25. Huang, J.; Li, Q.; Sun, D.; Lu, Y.; Su, Y.; Yang, X.; Wang, H.; Wang, Y.; Shao, W.; He, N. Biosynthesis of silver and gold nanoparticles by novel sundried *Cinnamomum camphora* leaf. *Nanotechnology* **2007**, *18*, 105104. [[CrossRef](#)]
26. Muhammad, D.R.A.; Praseptiangga, D.; Van de Walle, D.; Dewettinck, K. Interaction between natural antioxidants derived from cinnamon and cocoa in binary and complex mixtures. *Food Chem.* **2017**, *231*, 356–364. [[CrossRef](#)]
27. Ubaihulla, B.A.; Vadamar, R.; Vinodhini, A.; Fairrose, S.; Gomathiyalini, A.; Jabena, B.N.; Jabeen, S. Facile Green Synthesis of Silver Doped ZnO Nanoparticles Using Tridax Procumbens Leaf Extract and their Evaluation of Antibacterial Activity. *J. Water Environ. Nanotechnol.* **2020**, *5*, 307–320.
28. Chand, K.; Cao, D.; Fouad, D.E.; Shah, A.H.; Dayo, A.Q.; Zhu, K.; Lakhan, M.N.; Mehdi, G.; Dong, S. Green synthesis, characterization and photocatalytic application of silver nanoparticles synthesized by various plant extracts. *Arab. J. Chem.* **2020**, *13*, 8248–8261. [[CrossRef](#)]
29. Fouladi-Fard, R.; Aali, R.; Mohammadi-Aghdam, S.; Mortazavi-derazkola, S. The surface modification of spherical ZnO with Ag nanoparticles: A novel agent, biogenic synthesis, catalytic and antibacterial activities. *Arab. J. Chem.* **2022**, *15*, 103658. [[CrossRef](#)]
30. Jafarirad, S.; Taghizadeh, P.M.; Divband, B. Biosynthesis, characterization and structural properties of a novel kind of Ag/ZnO nanocomposites in order to increase its biocompatibility across human A549 cell line. *BioNanoScience* **2020**, *10*, 42–53. [[CrossRef](#)]
31. Verma, R.; Chauhan, A.; Shandilya, M.; Li, X.; Kumar, R.; Kulshrestha, S. Antimicrobial potential of Ag-doped ZnO nanostructure synthesized by the green method using Moringa oleifera extract. *J. Environ. Chem. Eng.* **2020**, *8*, 103730.
32. Kyomuhimbo, H.D.; Michira, I.N.; Mwaura, F.B.; Derese, S.; Feleni, U.; Iwuoha, E.I. Silver–zinc oxide nanocomposite antiseptic from the extract of *bidens pilosa*. *SN Appl. Sci.* **2019**, *1*, 1–17. [[CrossRef](#)]
33. Sorescu, A.-A.; Nuță, A.; Rodica, M.; Bunghez, I. Green Synthesis of Silver Nanoparticles Using Plant Extracts. In Proceedings of the 4th International Virtual Conference on Advanced Scientific Results, Zilina, Slovakia, 6–10 June 2016; pp. 10–16.
34. Ahmed, R.H.; Mustafa, D.E. Green synthesis of silver nanoparticles mediated by traditionally used medicinal plants in Sudan. *Int. Nano Lett.* **2020**, *10*, 1–14. [[CrossRef](#)]
35. Srikar, S.K.; Giri, D.D.; Pal, D.B.; Mishra, P.K.; Upadhyay, S.N. Green synthesis of silver nanoparticles: A review. *Green Sustain. Chem.* **2016**, *6*, 34–56. [[CrossRef](#)]
36. Xu, J.; Yang, Z.; Chen, S.; Wang, W.; Zhang, Y. Compatibility and Photocatalytic Capacity of the Novel Core@ shell Nanospheres in Cementitious Composites. *Catalysts* **2022**, *12*, 1574. [[CrossRef](#)]
37. Wang, J.; Hasegawa, T.; Asakura, Y.; Yin, S. Recent Advances in Ternary Metal Oxides Modified by N Atom for Photocatalysis. *Catalysts* **2022**, *12*, 1568. [[CrossRef](#)]
38. Costa, K.G.; Asencios, Y.J.O. Development of a Solid Catalyst Based on Pt Supported on Heterostructure (NaNbO₃/NaNb₃O₈/NiO) Applied to the Photodegradation of Phenol in Seawater. *Catalysts* **2022**, *12*, 1565. [[CrossRef](#)]
39. Rodionov, I.A.; Gruzdeva, E.O.; Mazur, A.S.; Kurnosenko, S.A.; Silyukov, O.I.; Zvereva, I.A. Photocatalytic Hydrogen Generation from Aqueous Methanol Solution over n-Butylamine-Intercalated Layered Titanate H₂La₂Ti₃O₁₀: Activity and Stability of the Hybrid Photocatalyst. *Catalysts* **2022**, *12*, 1556. [[CrossRef](#)]
40. Wang, K.; Liu, L.; Zhang, Y.; Su, J.; Sun, R.; Zhang, J.; Wang, Y.; Zhang, M. Synthesis and Visible Light Catalytic Performance of BiOI/Carbon Nanofibers Heterojunction. *Catalysts* **2022**, *12*, 1548. [[CrossRef](#)]
41. Janotti, A.; Van de Walle, C.G. Fundamentals of zinc oxide as a semiconductor. *Rep. Prog. Phys.* **2009**, *72*, 126501. [[CrossRef](#)]
42. Reynolds, D.; Look, D.C.; Jogai, B.; Litton, C.; Cantwell, G.; Harsch, W. Valence-band ordering in ZnO. *Phys. Rev. B* **1999**, *60*, 2340. [[CrossRef](#)]
43. Chen, Y.; Bagnall, D.; Koh, H.-J.; Park, K.-T.; Hiraga, K.; Zhu, Z.; Yao, T. Plasma assisted molecular beam epitaxy of ZnO on c-plane sapphire: Growth and characterization. *J. Appl. Phys.* **1998**, *84*, 3912–3918. [[CrossRef](#)]
44. Sriksaow, A.; Smith, S.M.; Uraisin, K.; Suttiponparnit, K.; Kongmark, C.; Chuaicham, C. Catalytic remediation of phenol contaminated wastewater using Cu-Zn hydroxide nitrate. *RSC Adv.* **2016**, *6*, 36766–36774. [[CrossRef](#)]
45. Chuaicham, C.; Inoue, T.; Balakumar, V.; Tian, Q.; Ohtani, B.; Sasaki, K. Visible light-driven ZnCr double layer oxide photocatalyst composites with fly ashes for the degradation of ciprofloxacin. *J. Environ. Chem. Eng.* **2022**, *10*, 106970. [[CrossRef](#)]
46. Gomez-Solís, C.; Ballesteros, J.; Torres-Martínez, L.; Juárez-Ramírez, I.; Torres, L.D.; Zarazua-Morin, M.E.; Lee, S.W. Rapid synthesis of ZnO nano-corncoobs from Nital solution and its application in the photodegradation of methyl orange. *J. Photochem. Photobiol. A Chem.* **2015**, *298*, 49–54. [[CrossRef](#)]
47. Rabell, G.O.; Cruz, M.A.; Juárez-Ramírez, I. Hydrogen production of ZnO and ZnO/Ag films by photocatalysis and photoelectrocatalysis. *Mater. Sci. Semicond. Process.* **2021**, *134*, 105985. [[CrossRef](#)]

48. Mousavi-Kouhi, S.M.; Beyk-Khormizi, A.; Amiri, M.S.; Mashreghi, M.; Yazdi, M.E.T. Silver-zinc oxide nanocomposite: From synthesis to antimicrobial and anticancer properties. *Ceram. Int.* **2021**, *47*, 21490–21497. [[CrossRef](#)]
49. Saqib, S.; Nazeer, A.; Ali, M.; Zaman, W.; Younas, M.; Shahzad, A.; Nisar, M. Catalytic potential of endophytes facilitates synthesis of biometallic zinc oxide nanoparticles for agricultural application. *BioMetals* **2022**, *35*, 967–985. [[CrossRef](#)]
50. Balakumar, V.; Manivannan, R.; Chuaicham, C.; Karthikeyan, S.; Sasaki, K. A simple tactic synthesis of hollow porous graphitic carbon nitride with significantly enhanced photocatalytic performance. *Chem. Commun.* **2021**, *57*, 6772–6775. [[CrossRef](#)]
51. Nagakawa, H.; Ochiai, T.; Ma, H.; Wang, C.; Zhang, X.; Shen, Y.; Takashima, M.; Ohtani, B.; Nagata, M. Elucidation of the electron energy structure of TiO₂(B) and anatase photocatalysts through analysis of electron trap density. *RSC Adv.* **2020**, *10*, 18496–18501. [[CrossRef](#)]
52. Unwiset, P.; Chen, G.; Ohtani, B.; Chanapatttharapol, K.C. Correlation of the Photocatalytic Activities of Cu, Ce and/or Pt-Modified Titania Particles with their Bulk and Surface Structures Studied by Reversed Double-Beam Photoacoustic Spectroscopy. *Catalysts* **2019**, *9*, 1010. [[CrossRef](#)]
53. Chuaicham, C.; Sekar, K.; Xiong, Y.; Balakumar, V.; Mittraphab, Y.; Shimizu, K.; Ohtani, B.; Dabo, I.; Sasaki, K. Single-step synthesis of oxygen-doped hollow porous graphitic carbon nitride for photocatalytic ciprofloxacin decomposition. *Chem. Eng. J.* **2021**, *425*, 130502. [[CrossRef](#)]
54. Krithiga, N.; Rajalakshmi, A.; Jayachitra, A. Green synthesis of silver nanoparticles using leaf extracts of *Clitoria ternatea* and *Solanum nigrum* and study of its antibacterial effect against common nosocomial pathogens. *J. Nanosci.* **2015**, *2015*, 928204. [[CrossRef](#)]

Disclaimer/Publisher’s Note: The statements, opinions and data contained in all publications are solely those of the individual author(s) and contributor(s) and not of MDPI and/or the editor(s). MDPI and/or the editor(s) disclaim responsibility for any injury to people or property resulting from any ideas, methods, instructions or products referred to in the content.